Journal of Applied Fluid Mechanics, Vol. 18, No. 3, pp. 567-584, 2025.
Available online at www.jafmonline.net, ISSN 1735-3572, EISSN 1735-3645.
https://doi.org/10.47176/jafm.18.3.2831

Studies on the Effect of Baffle Plates in Settling Chamber Performance by CFD and Experimental Analysis

S. Venkatesh[1†], R. Krishnaraj[2], P. M. Gopal[3] and V. Kavimani[3]

[†1] *Department of Mechanical Engineering, Sri Eshwar College of Engineering, Coimbatore, India*
[2] *Department of Mechanical Engineering, College of Engineering and Technology, Dambi Dollo University, Ethiopia*
[3] *Department of Mechanical Engineering, Karpagam Academy of Higher Education, Coimbatore, India*

† Corresponding Author Email: venkatesh.s@sece.ac.in

ABSTRACT

The performance of the settling chamber was examined in two scenarios in this study. In case 1, the settling chamber collection efficiency and flow characteristics were predicted without a baffle plate. In case 2, the settling chamber performance was predicted with the baffle plates. In case 2, two baffle plates were placed between the inlet and exit nozzle. The experimental set up was fabricated with the baffle plates to measure the performance. Moreover, the efficiency of the settling chamber was determined for the different inlet velocities. The Variable Frequency Drive (VFD) controller was adopted with the suction fan to vary the inlet velocity. The Reynolds Stress Model (RSM) was used to forecast the settling chamber flow characteristics. In cases 1 and 2, the best capture efficiency results were achieved at 2.5 m/s inlet velocity. The experimental study shows that the settling chamber gathering efficiency was 45% at 52.35µm. It is 44.4% higher than case 1. In CFD analysis, the settling chamber efficiency was 43%. The variation between the experimental and CFD results was 4.4%. The observations show that the pressure drop for the baffle plate setting chamber was increased 4.37 % compared to case1. The maximum settling velocity of the case 1 and case 2 chambers is 1.62 m/s and 2.81 m/s respectively. It indicates that the baffle plate chamber has highest setting velocity. Moreover, the hopper region has highest tangential velocity when introducing the baffle plate. The observations show that the radial velocity is increased in the rectangular wall region compared to hopper region due to the baffle plate.

Article History

Received May 7, 2024
Revised September 23, 2024
Accepted September 25, 2024
Available online January 1, 2025

Keywords:

Baffle plate effects
Flow pattern of particles
Pressure drop
Kinetic energy of the particles
Terminal settling velocity
Particle settling time

1. INTRODUCTION

Gravitational settling chambers are used to remove particles from a moving gas stream. When a stream of gas containing particles goes through this, the particles fall to the storage bin because of gravity (Flagan & Seinfeld, 1988). It is used as a pre-cleaner for high-end collectors like cyclones, wet scrubbers, electrostatic precipitators, etc. Moreover, it reduces the dust particles mixing with water (Scrubbing liquid) when it is connected with Venturi scrubber. It reduces the dust contamination in scrubbing water. It reduces the abrasive particles entering the high-efficiency collectors. The energy required for the recycling of scrubbing water is minimized by this settling chamber. Due to this, the efficiency of the high end collector is enhanced. Settling chambers are simple in construction, have a low pressure drop, and are low cost. However, a large space is required for installation, which is the major drawback (Bhattacharjee, 2003). There are three types of settling chambers: momentum chambers, simple growth chambers, and chambers with more than one tray. Settling chambers are widely utilised in powder metallurgy industries, food industries, and natural draught furnaces (Flagan & Seinfeld, 1988).

The settling chamber efficiency is related to the three important parameters, namely, the length, width, and height of the settling chamber. Usually, the dimensions of the settling chamber are designed based on the size of the particles to be collected. The literature report indicates that the increment in length of the settling chamber increases the collection efficiency because it increases the residence time of the particle. Therefore, in settling chamber design, the length of the chamber is always kept as large as possible. Moreover, large-length chambers are suitable to collect small

NOMENCLATURE

CD	drag coefficient of particle
dp	particle diameter
F_D	drag force
F_{ij}	production by system rotation
F_X	additional force
G_{ij}	buoyancy production
g	acceleration due to gravity
H	settling chamber duct height
K	turbulent kinetic energy
L	settling chamber length
N	number of baffle plates
ΔP	pressure drop
$P_{p,}$ ρ	particle density, Fluid or gas density
P_{ij}	stress production
R_e	Reynolds number
R_{ij}	Reynolds stress tensor
T	time
U	fluid phase velocity
u_{pi}	particle velocity
u	inlet air velocity
$(u_i' u_j')$	Reynolds stress tensor
u_i'	fluctuating velocity component
u_i, u_j, u_k	velocity component in corresponding direction
V_i	inlet velocity
x_{pi}	position of particles in i direction

Greek letters

μ	fluid viscosity
μ_t	turbulence viscosity
δ_{ij}	boundary layer thickness
ϵ	turbulent kinetic Dissipation rate

Abbreviation

RSM	Reynolds Stress Model
DRW	Discrete Random Walk
DPM	Discrete Phase Model
CFD	Computational Fluid Dynamics

particles. As per the literature, one of the authors investigated a 7 m length settling chamber (Nasiri & Abdolzadeh, 2019). Moreover, in that investigation, the height of the settling chamber was considered to be 3 m. As well, an increase in the width of the chamber decreases the throughput velocity of gas. Decreasing the throughput velocity of the gas increases its efficiency. Therefore, parameters such as the length and width of the chamber were always kept large during the design of the settling chamber. Moreover, the height of the settling chamber should be kept low when compared to its length. Since the increment in the height of the chamber reduces efficiency, few industries (medium-scale foundries) are utilising 7m x 7m x 15m settling chambers for better collection efficiency. For the installation of this kind of chamber, a large space is required.

In a few settling chambers, the baffle plates were utilised to divert the gas flow direction. Due to this, the particles are settled down in the bin by the gravitational force. Nasiri and Abdolzadeh (2019) was investigated the effect of inclined and curved baffle plates on the settling chamber performance with a single collection bin. Kolaitis and Founti (2002) applied an Eulerian-Lagrangian technique to examine the performance of a settling chamber without a vertical plate. Nieto et al. (2010) applied the finite volume method to test how well a new gravity chamber worked. Usually, an increment in the length of the settling chamber provides good collection efficiency. But it increases the fabrication cost and space requirements. The important design factors of this chamber are the height, length, and width of the chamber (Feather & Chen, 2003). The literature report indicates that the gas velocity must be kept low to control the re-entrained particles. The particle re-entrained due to its high velocity (Flagan & Seinfeld, 1988). The velocity with which the particles escape through the outlet of the chamber is called the pickup velocity. The low velocity is achieved inside the chamber by expanding the duct area. The particles have two velocity components when they enter the chamber, namely, horizontal velocity and vertical downward velocity due to gravity (Flagan & Seinfeld, 1988; Bhattacharjee, 2003). The horizontal velocity is recognized as the gas's throughput velocity, while the vertical velocity is identified as the terminal settling velocity. The length of time something stays in the settling space is also an important design factor. There must be enough time for the particle to be caught. Generally, the settling chambers are analysed by the nature of the flow, such as laminar flow and turbulent flow (Sahmel et al., 2015; Liu et al., 2019; Romblad et al., 2022).

The literature report indicates that the settling chamber gives reasonable collection efficiency when the particle sizes are greater than about 50 μm. Moreover, an increment in the chamber height, width, and length provides high efficiency when the particle sizes are small (less than 50 μm). However, an increment in the chamber size increases the space required for installation. It increases the fabrication cost and pressure drop. Moreover, high energy is required to operate the system. Therefore, in this work, two vertical baffle plates were positioned within the chamber to enhance the performance of the settling chamber without increasing the parameters, namely, the length, width, and height of the chamber. In this study, the performance of the settling chamber is analysed with and without a baffle plate by the experimental and CFD analysis.

2. GEOMETRY DETAILS

The difference between the first design and the second design is highlighted in green in Fig. 1. The main difference between the first and second designs is the baffle plates. Moreover, in the experimental setup, the VFD controller has been adopted to vary the speed of the blower. It is shown in Fig. 2. In this work, the square-type settling chamber was modelled in the PTC-Creo 3D modelling package. In this work, the first model was developed with baffle plates. Another model was

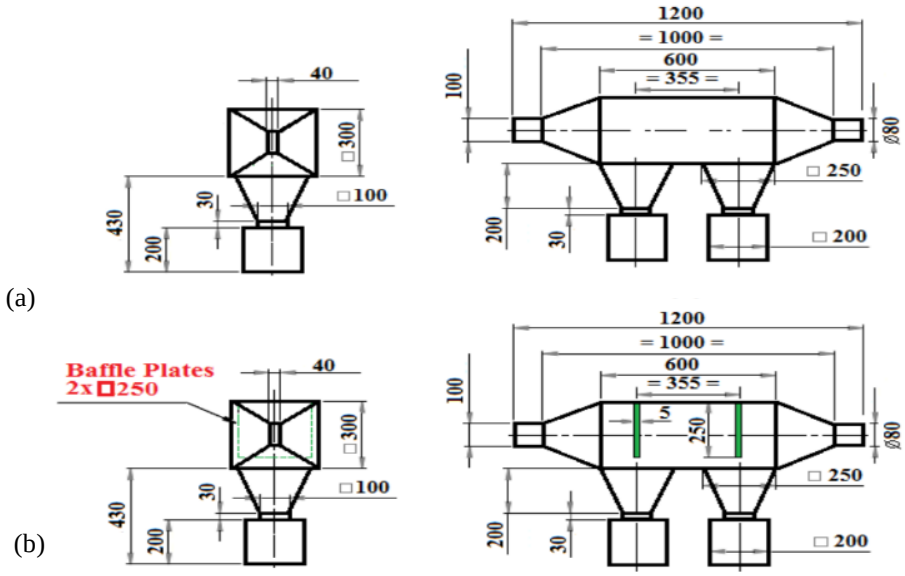

Fig. 1 Settling chamber geometry a) with baffle plate b) without baffle plate (All the dimensions are in mm)

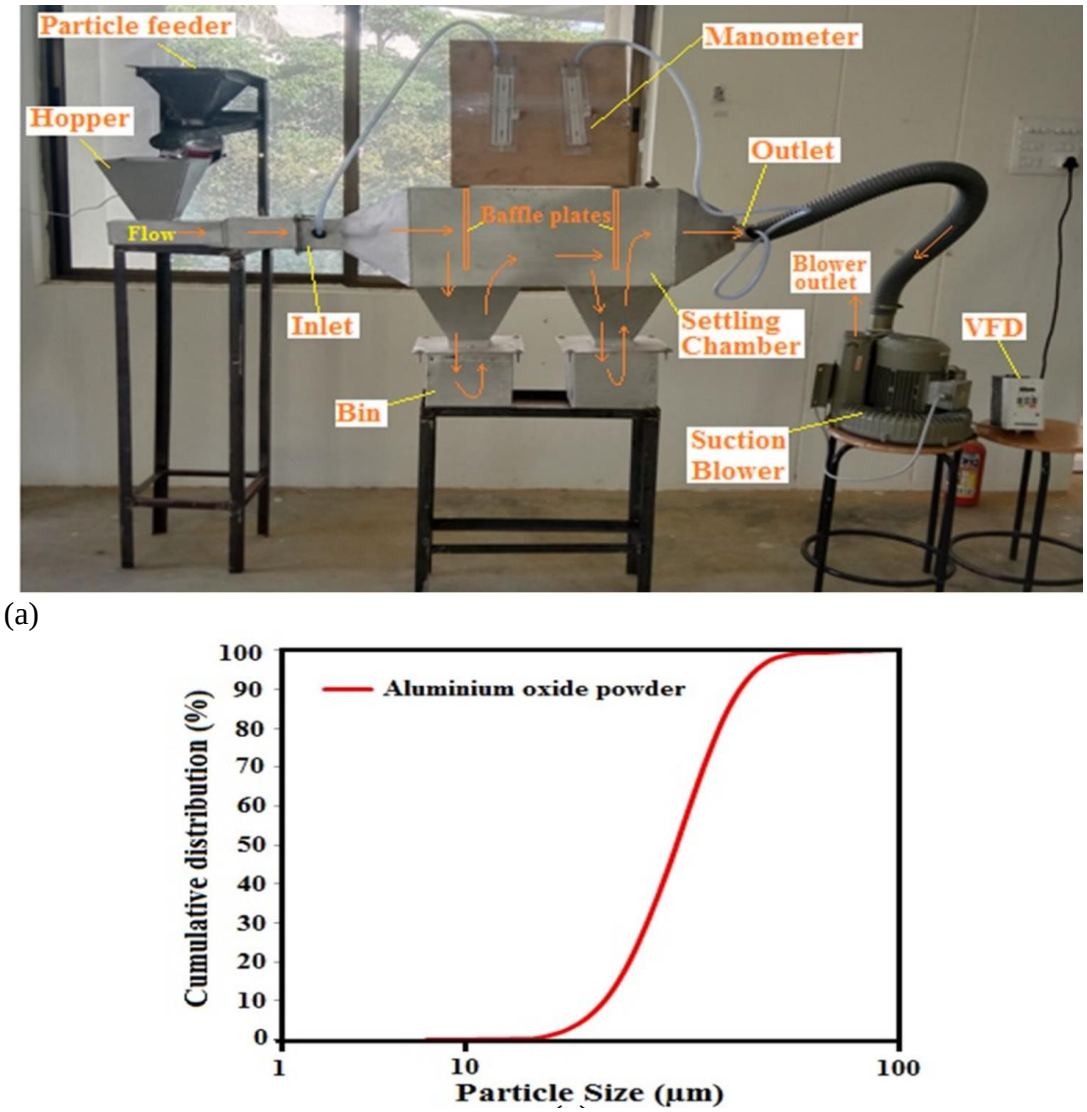

Fig. 2. a) Settling chamber with baffle plate experimental setup b) particle size distribution (Al_2O_3)

developed without baffle plates. The size of the baffle plate is 250 mm × 250 mm × 5 mm. The space between the two baffle plates is 355 mm. The width and height of the settling chamber are 300 mm × 300 mm. The length of the settling chamber is twice its width. The length of the settling chamber is 600 mm.

In this settling chamber, a divergent type of gas inlet duct was connected on the left side. The right side of the settling chamber was linked to the convergent-type gas outlet duct. The point of entry was in the shape of a square, and the exit was in the shape of a circle. The intake port size is 100 mm × 40 mm. The exit port is Ø80 mm in size. Two collection bins were spaced out at the same distance at the bottom of the truncated pyramid hoppers. The total length of the settling chamber was 1200 mm (inlet to exit nozzle). According to the Stokes law, Eqs. 1 and 2 were applied to determine the collection efficiency (η) and terminal settling velocity (v_t) in the settling chamber (Flagan & Seinfeld, 1988). According to the Eq. 1, the settling chamber's efficacy is proportional to the length (L), particle density, particle diameter, and number of baffle plates (N). The efficiency is also indirectly related to the height (H) and the gas velocity (u). Eqs. 1 and 2 are used to calculate the theoretical efficiency and terminal settling velocity of the settling chamber based on the available particle size. In this work, the required size of Al_2O_3 powder has been prepared through the ball milling process. The average mean particle size of 52.35 μm (ρ_p = 3950 kg/m^3) was used for experimentation. For a settling chamber without a baffle plate (Flagan & Seinfeld, 1988), we used N = 1 in Eq. 1. The second case provided two baffle plates. According to the settling chamber design procedure (Flagan & Seinfeld, 1988), the number of baffle plates for a baffle plate settling chamber should be N = 3 (N = 1 + number of baffle plates). We have estimated the particle's efficiency and settling velocity using the following parameters: L = 0.6 m, g = 9.81 m/s^2, μ = 1.8x10^{-5} kg/ms, u = 2.5 m/s, and H = 0.3 m. According to the calculation, the settling chamber efficiency without a baffle plate is 23%, and the particle settling velocity is 0.32 m/s. The settling chamber efficiency with the baffle plate is 52%, and the particle settling velocity is 0.96 m/s. Placing two baffle plates inside the chamber increases the particle settling velocity by three times, as the setting velocity multiplies N = 3. (A detailed discussion is provided in Fig. 12 and 13). Eq. 1 shows that an increment in the length and number of baffle plates increases the collection efficiency.

Moreover, an increment in the inlet velocity and height decreases the efficiency. As per the Stokes law, the terminal velocity is directly proportional to the efficiency. An increase in terminal settling velocity increases collection efficiency. Furthermore, the inclusion of additional baffle plates enhances the system's efficiency by prolonging the duration of particle retention and reducing the rate of particle uptake. The design process says that the inlet velocity of the gas should be maintained between 1.5 and 3 m/s (Sinnott, 2005). Figure 1 shows the measurements of the settling chamber, which were used to make it.

$$\eta = 1 - exp\left(-\frac{L\rho_p g d_p^2 N}{18\mu\bar{u}H}\right) \quad (1)$$

$$v_t = \frac{\rho_p g d_p^2}{18\mu} \quad (2)$$

3. EXPERIMENTAL SETUP

The part details are clearly mentioned in Fig. 2. The flow direction is marked with arrows from the inlet to the outlet. In this experiment, the flow is started at the inlet. It means the air is drawn from the atmosphere through the inlet of the settling chamber by a suction blower. The direction of the air flow is changed to the collection bin due to the vertical baffle plates when the air enters the rectangular chamber. Afterwards, the air is moved through the outlet of the settling chamber to the suction blower. Then, the air exits the atmosphere through the exit port of the suction blower. The entire chamber was fabricated from the mild steel sheet with a thickness of 2 mm. In this settling chamber, a particle feeding hopper was connected to the inlet section. The suction fan's inlet and the settling chamber's exit were linked by a flexible hose. The fan has two openings. One port is used to take in air, and the other port is used to send air into space. The suction face of the blower was connected with the outlet port of the settling chamber. The suction blower is operated by a 2-hp motor (220V–240V, Single phase). The flow rate at the suction port's entry point was 210 m^3/hr. The upper limit speed of the blower was 2800 rpm. Moreover, the blower speed was controlled by a VFD. The speed of the blower can be adjusted by the VFD controller from 0 to 2800 rpm.

In this experimental setup, the entire chamber was fabricated from a mild steel sheet with a thickness of 2 mm. This thickness of material provides the settling chamber with good strength and stiffness. Moreover, a proper gasket secures all components to the settling chamber, preventing air leakage during operation. This setup uses a side channel blower, which generates less vibration than other suction blowers. Furthermore, a rigid frame securely seated the settling chamber. Additionally, we conducted an uncertainty analysis to prevent measurement errors due to overconfidence in the experimental analysis. The overall uncertainty value for this experimental analysis is ± 0.097. It indicates that the measuring instruments and measurement methods used in this analysis produce significant results.

The input velocity of the air was measured in the settling chamber using a digital anemometer at various blower speeds. At the bottom of the dust collecting hoppers, two collection bins were linked. In this settling chamber, two manometers were used to record the variation in pressure between the entry and exit nozzle. The design process says that the settling chamber should be run at 1.5 to 3 m/s (Sinnott, 2005). In this experiment, the entrance velocity was raised from 1.5 m/s to 4 m/s so that the pressure drop at each velocity could be measured. It was done by the changing of blower speed through VFD. With respect to the entry velocity of air, the pressure drop was augmented from 107.8 Pa to 186.3 Pa (11 mm of H_2O to 19 mm of H_2O). The chamber

Table 1 Uncertainty analysis report

Equipment name	Measuring parameter and unit	Accuracy	Uncertainty
Laser particle size analyzer	Particle size (µm)	±0.01 µm	$\pm 1.55e^{-04}$
Anemometer	Velocity (m/s)	± 0.6 m/s	±0.064
Manometer	Pressure (mm of H_2O)	±1 mm of H_2O	±0.054
Settling chamber	Efficiency (%)	±4 %	±0.049

efficacy was measured using the aluminium oxide (Al_2O_3) powder (density = 3950 kg/m^3). Furthermore, the average mean particle size of 52.35µm was used to calculate collecting efficiency. The ball milling technique was applied to prepare the desired powder size. The particle size was measured using a laser particle size analyser (Jinon Winner, 2005A). The particles were injected at 20 g/s. Moreover, the blower was run at 5s to monitor the particle re-entrainment. In each test, 200 g of particles were injected to measure the efficiency of the baffle plate settling chamber. At 52.35 µm, the collecting efficacy of the settling chamber was tested at various velocities (1.5, 2, 2.5, 3, 3.5, and 4 m/s). The efficiency was augmented when the velocity was elevated from 1.5 m/s to 2.5 m/s. Further increment in the velocity (beyond 2.5 m/s) reduces efficiency. The settling chamber's highest efficiency was found to be 45% at 2.5 m/s. The sample has been taken out of the collection bin in order to confirm the sizes of the particles that were collected. The particle size analyser has since evaluated this sample size. Figure 2a displays the particle size distribution curve. According to this report, the sample's measurements are D90 = 68.231 µm, D10 = 38.47 µm, and Dav = 52.35 µm. The efficiency was measured by the ratio of weighing the collected powder particles in two bins to the introduced powder particles. It was observed that 74 g of particles were settled in the first collection bin and 22 g of particles were collected in the second collection bin. Totally, 96 g of particles were collected by two collection bins, and the remaining 104 g escaped to the atmosphere through the blower outlet port. (The comparison results and error bar reports are provided in Section 5.4)

3.1 Uncertainty Analysis

The purpose of conducting uncertainty analysis is to avoid overconfidence errors in the experimental setup measurement process. In this experimental analysis, different types of measuring instruments were utilised to measure the various parameters. Those measuring instruments have high precision and reliability. However, to avoid errors during the measurement process, this analysis was conducted. It helps to compare the results obtained from various instruments. This analysis gives a report about measured values that lie within the expected range. This analysis employs a statistical method to determine the standard deviation, also known as the standard error. This section provides detailed steps from step 1 to step 7. It indicates that the measuring instruments and measurement methods used in this analysis produce significant results.

The uncertainty analysis report is given in Table 1. The measuring equipment, such as a laser particle size analyzer, anemometer, manometer, and settling chamber, is utilized for conducting the uncertainty analysis.

The overall uncertainty value for this experimental analysis is ± 0.097. In this analysis, three tests have been conducted on each equipment. For conducting the uncertainty analysis, the following steps are applied:

Step 1: Determine the measuring parameter values by conducting three tests for each equipment.

Step 2: Determine the maximum and minimum value from the test.

Step 3: The accuracy of the particular measuring equipment is added to the maximum value to find out the maximum limit. Then the accuracy is subtracted from the minimum value to find out the minimum limit.

Step 4: Calculate the average value from the maximum and minimum limits.

Step 5: Calculate the subtraction values by subtracting each test value from the average value from step 4.

Step 6: Calculate the sum of squares of the subtraction value from step 5 and find out its average.

Step 7: Calculate the uncertainty value by taking the square root of the average value from step 6 and dividing it by the average value from step 4.

4. CFD ANALYSIS

4.1 Turbulence Model Equations

The Reynolds number (Re) was determined before starting the simulation to anticipate whether the stream is turbulent or laminar (Liu et al., 2019; Nasiri & Abdolzadeh, 2019). For predicting the Re in the settling chamber, the following equation was proposed (Flagan & Seinfeld, 1988).

$$Re = \frac{H\tilde{u}\rho}{\mu} \tag{3}$$

The following parameters were considered for calculating the Re: The settling chamber duct height (H) = 0.3 m, velocity = 2.5 m/s (the minimum velocity required to operate the settling chamber), density = 1.293 kg/m^3, and dynamic viscosity = 1.8×10^{-5} kg/ms (air). The predicted Re for the rectangular duct settling chamber was 53,875. It indicates that the flow is turbulent. In past decades, few researchers applied k-ε model to solve the turbulence flow in settling chambers (Liu et al., 2019; Nasiri & Abdolzadeh, 2019). Presently, most researchers

use the RSM to solve multiphase flow applications due to its accuracy (Raoufi et al., 2009; Safikhani et al., 2011a; Su et al., 2011; Elsayed & Lacor, 2012; Fatahian et al., 2018; Wasilewski et al., 2020). The RSM is a most suitable model for solving complex flow problems. The literature reports show that the RSM is suitable to solve sudden changes in flow direction. Moreover, it produces accurate results in strong swirling flows, rotating flows, and streamline curvature flows. The RSM utilises seven additional transport equations to solve the 3D flows. In addition, the RSM produces accurate results in tangential, axial, and radial velocity components. It produces accurate results in pressure-velocity coupling compared to the other turbulence models (Griffiths & Boysan, 1996; Fluent, 2004; Chuah et al., 2006; Elsayed & Lacor, 2010; Safikhani et al., 2011a; Venkatesh et al., 2017, 2021; Patro et al., 2023). As per the literature report, other two equation models, such as the k-ε model and the k-ω model, failed to produce accurate results in complex flow problems. Therefore, RSM is applied in this simulation. Accordingly, RSM was used in this study to examine the performance of the settling chamber.

The mass and momentum in an incompressible Newtonian flow can be written as (Fluent, 2004)

$$\frac{\partial \overline{u_i}}{\partial x_i} = 0 \tag{4}$$

$$\frac{\partial \overline{u_i}}{\partial x_i} + \overline{u_j}\frac{\partial \overline{u_i}}{\partial x_j} = -\frac{1}{\rho}\frac{\partial \bar{P}}{\partial x_i} + v\frac{\partial^2 \overline{u_i}}{\partial x_j \partial x_j} - \frac{\partial}{\partial x_j}R_{ij} \tag{5}$$

Where,

$$R_{ij} = \overline{u_i' u_j'} \tag{6}$$

Where, the u_i' can be written as (Fluent, 2004)

$$u_i' = u_i - \overline{u_i} \tag{7}$$

The turbulence stress components can be determined by the differential transport equations of RSM (Fluent, 2004):

$$\frac{\partial}{\partial t}R_{ij} + \overline{u_k}\frac{\partial}{\partial x_k}R_{ij} = \frac{\partial}{\partial x_k}\left(\frac{v_t}{\sigma^k}\frac{\partial}{\partial x_k}R_{ij}\right) - \left[R_{ik}\frac{\partial \overline{u_j}}{\partial x_k} + R_{ik}\frac{\partial \overline{u_i}}{\partial x_k}\right] - C_1\frac{\varepsilon}{K}\left[R_{ij} - \frac{2}{3}\delta_{ij}K\right] - C_2\left[P_{ij} - \frac{2}{3}\delta_{ij}P\right] - \frac{2}{3}\delta_{ij}\varepsilon \tag{8}$$

Where P_{ij} can be computed from Eq. (9)

$$P_{ij} = -\left[R_{ik}\frac{\partial \overline{u_j}}{\partial x_k} + R_{jk}\frac{\partial \overline{u_i}}{\partial x_k}\right],\ P = \frac{1}{2}P_{ij} \tag{9}$$

The turbulence dissipation rate, ε can be written as:

$$\frac{\partial \varepsilon}{\partial t} + \overline{u_j}\frac{\partial \varepsilon}{\partial x_j} = \frac{\partial}{\partial x_j}\left[\left(v + \frac{v_t}{\sigma^\varepsilon}\right)\frac{\partial \varepsilon}{\partial x_j}\right] - C^{\varepsilon 1}\frac{\varepsilon}{K}R_{ij}\frac{\partial \overline{u_i}}{\partial x_j} - C^{\varepsilon 2}\frac{\varepsilon^2}{K} \tag{10}$$

The fluctuating kinetic energy (K), can be written as (Fluent, 2004)

$$K = \frac{1}{2}\overline{u_i' u_i'} \tag{11}$$

The values of constants are $\sigma^k = 1$, C_1=1.8, C_2=0.6, $\sigma^\varepsilon = 1.3$, $C^{\varepsilon 1}$= 1.44 and $C^{\varepsilon 2}$= 1.92.

4.2 Discrete Phase Model

In the present simulation, the particle shape was considered as spherical. Therefore, the drag coefficient was solved by the Morsi and Alexander (1972) correlation. In this simulation, the discrete random walk (DRW) method was applied to solve elements turbulence dispersion (Liu et al., 2019; Nasiri & Abdolzadeh, 2019). The changing velocity field was divided into piecewise constant functions of time in DRW (Fluent, 2004). Their unsystematic value leftovers stable for the usual eddy lifetime (Te) (Fluent, 2004). In this situation, the ith-direction prompt velocity can be written as:

$$u_i' = \zeta\sqrt{\overline{u_i' u_i'}} \tag{12}$$

For RSM, $T_e = 0.3\ K\varepsilon$ (13)

In this work, the multiphase flow is activated during the simulation through the discrete phase model (DPM) approach because there are two phases available. The first phase is considered air (the fluid phase), and the second phase is considered particles. In this simulation, the particles are drawn into the settling chamber by the air. In CFD analysis, two approaches are available to model the multiphase flow. The first one is the Eulerian-Eulerian approach, and the second one is the Eulerian-Lagrangian approach. In the first method, all the phases are considered a continuous medium with properties similar to those of a fluid. This method follows the interpenetrating continua concept. In the Eulerian-Lagrangian approach, the liquid phase is treated as a continuum phase. Moreover, the Lagrangian particle trajectory analysis is applied to track the particles, or discrete phase (DP). One-way coupling was utilised in the numerical model. In this simulation, air was treated as a permanent stage. The scattered DP was handled as particles. The gas phase was solved using the Navier-Stokes equation (steady-state). The particle pathways were tracked by the Lagrangian frame. To follow discrete elements through a continuum fluid, DPM was used. In the detached phase, the forces of gravity and drag are included. The particles' interface has been abandoned. The DP was solved using the Runge-Kutta method (Raoufi et al., 2009; Safikhani et al., 2011b; Su et al., 2011; Fatahian et al., 2018). The following assumptions have been considered during the simulation (Fluent, 2004)

- This simulation assumes an isotropic flow of turbulence. It indicates that the properties are the same at all points and directions.
- Moreover, the RSM can use gradient diffusion to model turbulent fluxes.
- Model coefficients are constant. The model coefficients remain constant regardless of fluctuations in the flow. The small-scale turbulence is assumed to be in equilibrium.
- The numerical discretization did not account for non-turbulent fluctuations.

In DPM, the following assumptions were considered according to the Fluent 2004 manual

- The fluid phase is assumed to be a continuum (Zhao et al., 2006).
- A 10-12% volume fraction
- Assume the situation is completely elastic.
- The intake received a modest injection of particles.
- The inlet receives the spherical-shaped particles with a uniform diameter, injected in a normal plane.
- In real time, the particles are colliding with each other, but the DPM assumes that the particles are not colliding with each other (Zhao et al. 2006).
- There is no interaction between particles and the settling chamber wall.
- The gas phase was solved using the Navier-Stokes equation (steady-state).
- The lagrangian frame tracked the particle pathways.
- The drag coefficient is constant.
- Saffman force, Brownian motion, and magnetic forces are neglected (Fluent, 2004).

$$\frac{du_{Pi}}{dt} = F_D(u_i - u_{Pi}) + \frac{g_x(\rho_P - \rho)}{\rho_P} \tag{14}$$

$$\frac{dx_{Pi}}{dt} = u_{Pi} \tag{15}$$

$$F_D = \frac{18\mu}{\rho_P d_P^2}\frac{C_D R_e}{24} \tag{16}$$

$$R_e = \frac{\rho d_P |u_P - u|}{\mu} \tag{17}$$

4.3 Boundary Conditions and Settings

Ansys Fluent 15.0 executed the settling chamber simulation. The settling chamber has a rectangular inlet. In the experimental setup, the ring blower draws the air from the atmosphere to the settling chamber through the inlet port. The vacuum develops at the inlet port of the settling chamber when the ring blower is operated. Therefore, the air from the atmosphere is entering the settling chamber with a particular suction velocity. This suction velocity has been measured by the digital anemometer. The same velocity input is given as the boundary condition in the CFD simulation. Therefore, the velocity inlet boundary condition is provided in the inlet port. The velocity inlet condition was provided for this section with a turbulence intensity of 5%. The particle velocity and gas velocity are the same at the settling chamber inlet. The settling chamber has a circular outlet, the pressure outlet condition was provided for this section. The remaining settling chamber walls were configured as no slip wall conditions. The trap condition was provided in DPM in the two collection bins, and the escape condition was presented in the settling chamber outlet. To track the particles in DPM, the reflection condition was applied to all of the settling chamber's walls. Air has a dynamic viscosity of 1.8×10^{-5} kg/ms and a density of 1.293 kg/m^3. The settling chamber's inflow velocity was 2.5 m/s. The contour plots are generated at a rate of 2.5 m/s. Density of Al_2O_3 was provided as 3950 kg/m^3 in DPM. The Al_2O_3 mass flow rate was given as 20 g/s (the same as in the experimental study). Eq. 18 was used to calculate the separation performance of the settling chamber. The scaled residual for checking convergence accuracy was reported as 10^{-4} (Fluent, 2004). The SIMPLE approach was used to work out the pressure-velocity coupling. A second-order upwind scheme was applied to work out momentum, turbulence dissipation rate, and turbulence kinetic energy (Launder & Spalding, 1983; Launder & Shima, 1989). The SIMPLE scheme is highly suitable for solving complex and multi-phase flow problems. It is an implicit method that is highly stable compared to other explicit methods. It results in a precise pressure-velocity coupling. It requires less iteration to produce the results. Therefore, this scheme is chosen in this simulation. The second-order upwind scheme has higher accuracy compared to the first-order upwind scheme when solving complex flow problems. It reduces numerical diffusion and enhances the simulation's stability. Moreover, it is suitable for solving high Reynolds number flows. Therefore, this scheme is chosen in this simulation. The Courant number (CFL) for the current simulation (velocity 2.5 m/s, cell size 3 mm) was found to be 0.83. For the turbulence model, the Fluent manual recommends a CFL of 0.5 to 1 (Fluent, 2004). The total flow time was 5s. The time step size was specified as 0.001 s, with a total of 20 iterations per time step. The total number of time steps was determined to be 5000. The stable condition was monitored by opening the separate windows for pressure, velocity, and residuals. The stable condition in the results started at 4.7 s. The calculation was completed in 5s. The results were averaged over 4.7s to 5s

Efficiency $\eta\,(d_p)$ =

$$\frac{No.of\ Particles\ trapped}{No.of\ particels\ injected - No.of\ particles\ incomplete} \tag{18}$$

4.4 Mesh Details and Grid Independence Study (GIS)

The settling chamber model was developed by the PTC-Creo package, and it was exported to Ansys Fluent for grid generation and simulation. In CFD analysis, the accuracy of the results highly depends on the number of elements developed in the component. An increase in the number of elements produces highly accurate results in simulation. As well, an increment in the number of elements increases the computational time. For this purpose, initially, a coarse grid is developed for simulation to check the accuracy. Afterwards, the number of elements is gradually increased by adjusting the mesh size to generate the fine grids for analysing the grid independence report. The number of elements developed for the without baffle plate settling chamber is 190,540. The number of elements developed for the baffle plate settling chamber is 235,866. This is the maximum number of elements that can be developed in the present simulation. Beyond this limit, the accuracy is the same. At the same time, the computational time is increased when increasing the mesh size beyond this limit. Therefore, the above-mentioned number of elements is considered in the present simulation. The

Table 2 Settling chamber GIS results

Grid	No of elements (with plate)	Pressure drop (Pa)	No of elements (without plate)	Pressure drop (Pa)
G1	121,813	140.45	105,716	134.22
G2	148,387	140.82	124,914	134.7
G3	161,758	140.9	143,263	134.86
G4	188,245	141.6	164,086	135.35
G5	235,866	141.6	190,540	135.4

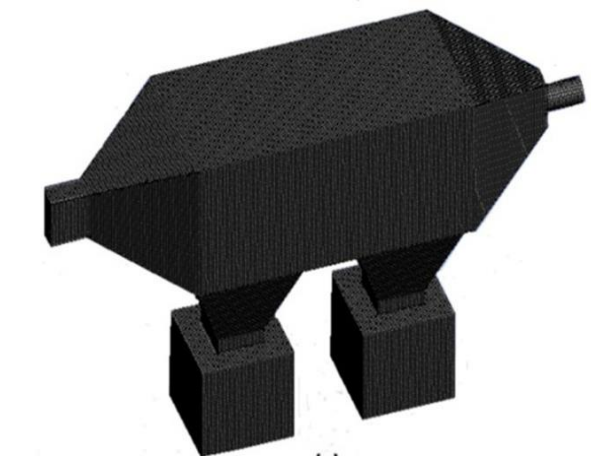

(a)

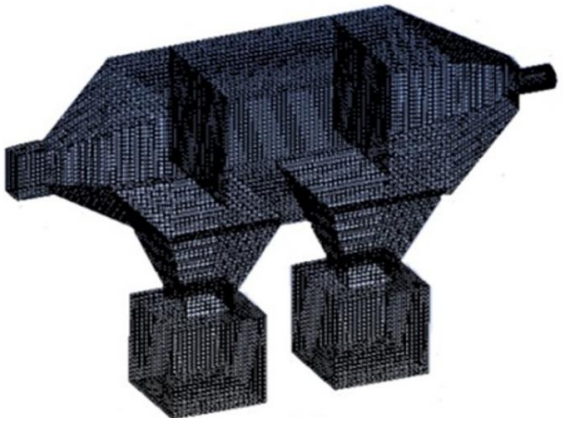

(b)

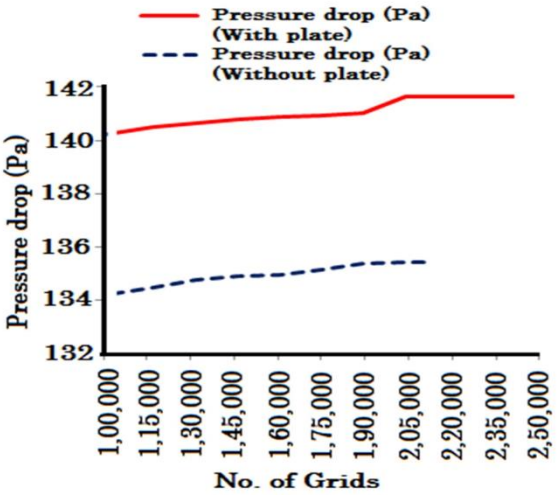

(c)

Fig. 3 Settling chamber grid a) without baffle plate b) with baffle plate c) No. of grids vs pressure drop

hexahedral grid was developed for the settling chamber which is shown in Fig. 3. The minimum cell dimension was 3 mm. A high smoothing option was given in the hexahedral mesh to develop a fine mesh. For executing the GIS, five sets of grids were developed. For each set of grids, the pressure drop was estimated as per the boundary condition mentioned (at 2.5 m/s) in the preceding part. The GIS outcomes are given in Table 2. The refinement ratio (fine to mid) for the baffle plate chamber was 1.45. The refinement ratio for the baffle plate chamber was 1.33. The obtained refinement ratio satisfies Richardson's theory (Roache, 1994; Slack et al., 2000). The GIS report indicates that the developed grid was suitable for simulation. For obtaining the accuracy in convergence and avoiding uncertainty in computational simulation, the highest number of grid elements was chosen for executing the simulation (Rajmistry et al., 2017; Houben et al., 2016). In this simulation, the near-wall modelling method has been applied to treat the near-wall turbulence effects. Initially, the viscosity-affected region was identified in the settling chamber. Afterwards, 20 layers of fine mesh were created in this viscosity-affected region to solve the turbulence quantities and mean velocity with a growth rate of 1.2. The obtained y+ value next to the wall cell is 0.92. The fluent manual suggests that the y+ value must be less than 4 for the viscosity-affected region. It confirms that the developed mesh provides good accuracy in simulation.

4.5 CFD Settings Validation

Kolaitis and Founti (2002) applied k-ε model to simulate the horizontal flow settling chamber in the past decade. In that research, perlite particles were used for simulation. The settling chamber was simulated in that study with a particle density of 100 kg/m^3. The mass flow rate considered in that study was 0.1553 kg/s. The particle size employed in that study was 2.5 mm. Furthermore, the study found that raising the inlet velocity advances the fraction of particles escaping through the exit nozzle. The dimensions of the settling chamber simulated in that study were 2.2 × 1 × 0.7 m. For validating the CFD settings in the present study, the same model was developed in PTC-creo.

Moreover, it was simulated with the above mentioned parameters using the RSM instead of k-ε model. The validation results for the k-ε model and RSM are provided in Fig. 4a. The validation result indicates that the present CFD settings applied in this work are suitable to simulate the settling chamber. In Fig. 4b, the deviation of results between the k-ε model and RSM is provided. The result indicates that the deviation between the k-ε model and RSM is 4.5%. It concludes that the RSM provides 4.5% accurate results when compared to the k-ε model.

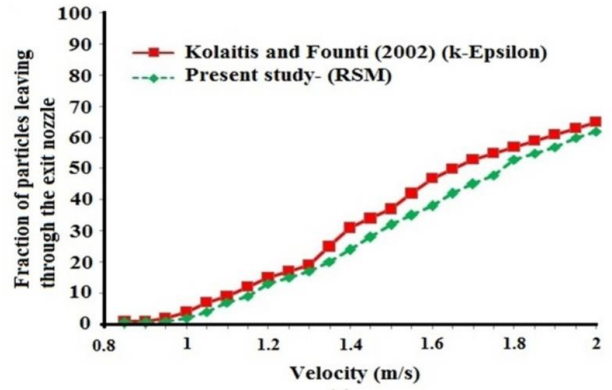

(a)

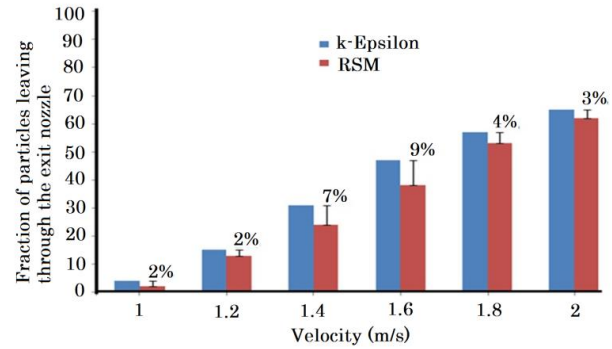

(b)

Fig. 4 CFD settings validation: a) Velocity vs Fraction of particles escape b) % of deviation in results for k-ε and RSM

5. RESULTS AND DISCUSSION

5.1 Settling Chamber Pressure Contours

Figure 5 depicts the pressure contours (time-averaged profiles) for the chambers without and with baffles. Figure 6 depicts the pressure drop findings for various input velocities. Two sectional views were created in this contour plot to better comprehend the flow characteristics. The first sectional view (Front) was obtained in the Y-Z plane at the centre of the settling chamber, where X = 0. At the halfway of the inlet and outflow portions, the second sectional view (Top) was obtained. This sectional view was obtained on the X-Z plane, with Y=0. The pressure increased from the entrance portion to the end of the outflow duct, as seen by these contour graphs. The outcomes of the settling chamber pressure drop prove that increasing the intake velocity increases the pressure drop. Furthermore, when compared to the top part or rectangular duct in both circumstances, the settling chamber collection bin has reduced pressure drop. Furthermore, in both circumstances, the first collection bin has a lower pressure drop than the second one. Two baffle plates were used within the settling chamber in this work. The contour plots demonstrate that when the baffle plate was inserted into the settling chamber, the pressure drop increased.

Figure 6 shows a comparison of CFD and experimental data. In experimental and CFD simulations, the settling chamber pressure drop was calculated at six

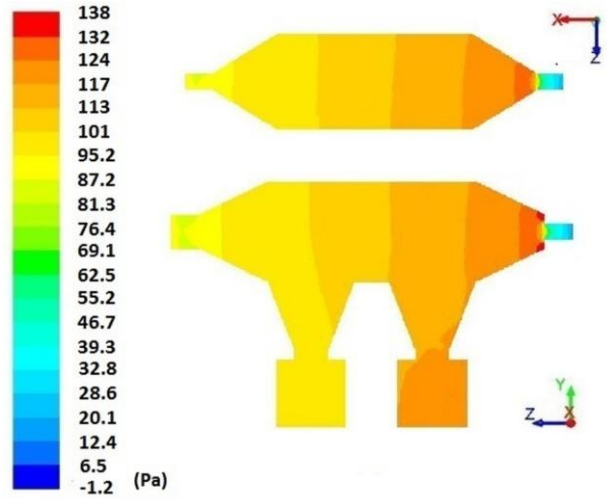

(a)

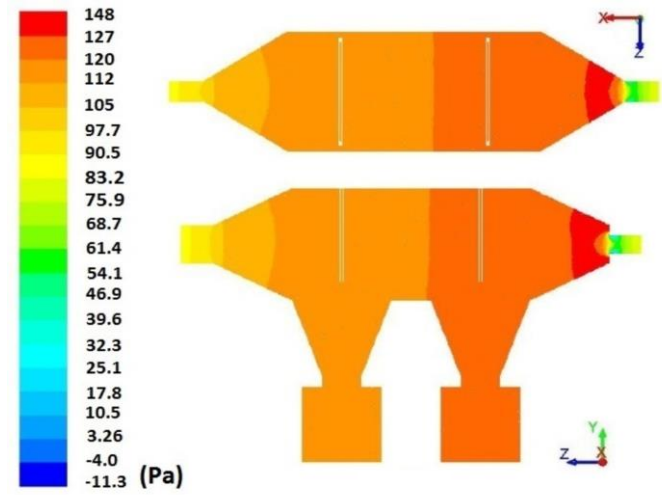

(b)

Fig. 5 Pressure contours (time averaged profiles): a) Without baffle plate b) With baffle plate

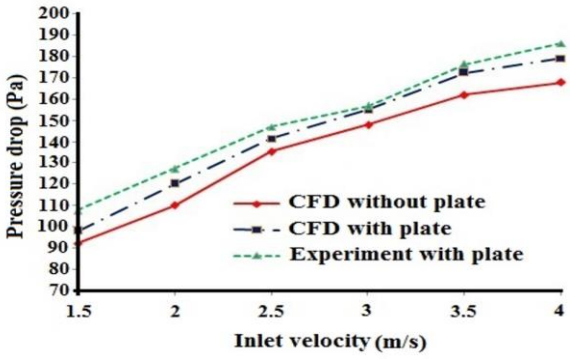

Fig. 6 Pressure drop results for different inlet velocity

different velocities (1.5, 2, 2.5, 3, 3.5, and 4 m/s). The maximum pressure drop for running the settling chamber was 250 Pa recommended by the design procedure (Nasiri & Abdolzadeh, 2019). The pressure drop at 2.5 m/s was 135.4 Pa for without baffle plate chamber. Furthermore, the pressure drop (CFD) for the two baffle

plate settling chamber was 141.6 Pa at 2.5 m/s. When the vertical baffle plates were installed inside the chamber, the settling chamber pressure drop rose by 4.37%. The experimental outcomes confirm that the pressure drop at 2.5 m/s (with baffle) was 147.1 Pa (15 mm of H_2O).

The deviation between experiment and CFD results is 3.8% for the baffle plate chamber. The settling chamber (without baffle) pressure drop was increased from 92.2 Pa to 168 Pa, corresponding to an increment in velocity (1.5 to 4 m/s). On the other hand, the settling chamber (with baffle) pressure drop was increased from 98.1 Pa to 179.3 Pa, corresponding to an increment in velocity (1.5 to 4 m/s). In experimental analysis, the suction blower and manometers have been connected with tubes, joints, and connectors. These tubes, joints, and connecting ports create minor losses in the flow. Moreover, the settling chamber fabrication material produces losses in flow due to the roughness factor. However, in CFD analysis, those kinds of minor losses are not considered during the simulation. Therefore, a small amount of deviation between the CFD and experimental results occurred. The maximum and minimum deviations between the experimental and CFD simulations are 5.8% and 1.1%, respectively. These deviations are within an acceptable range.

The divergent duct connected the settling chamber's inlet to the rectangular chamber's left side. When the air entered the divergent duct, the velocity decreased and the pressure increased towards the rectangular chamber. The contour plots show the same thing. Moreover, the length of the rectangular chamber is high when compared to the ducts attached at the inlet and outlet. Additionally, we connected duct-type hoppers to collection bins at the bottom of the rectangular chamber. This led to a flow diversion within the settling chamber. This flow diversion increases the turbulence and friction. As a result, the settling chamber experienced an increase in pressure. The contour plots clearly demonstrate an increase in pressure in the rectangular chamber and hoppers compared to the inlet. Moreover, the baffle plates create an obstruction in the flow between the inlet and exit ports. Usually, obstruction in the flow reduces the flow area and increases the pressure drop. In figure 5b, it can be noted that the wave is created between the plate and convergent duct due to the first baffle plate. Furthermore, these two baffle plates redirect the flow towards the hoppers and dust bin at a high terminal settling velocity. Therefore, the turbulence and boundary layer separation occurred inside the chamber, which increased the pressure drop. Simultaneously, the convergent duct diverts the flow towards the second hopper on the right side. It creates turbulence inside the chamber. Figure 5 clearly demonstrates this effect in the right side duct. As a result, there was an increase in the pressure drop.

5.2 Settling Chamber Velocity Contours

The settling chamber velocity contours are given in Fig. 7 (without baffle plate) and Fig. 8 (with baffle plate). In settling chamber case 1 (without baffle plate), the axial velocity was decreased at the inlet duct or divergent duct. Further, the axial velocity was increased towards the exit

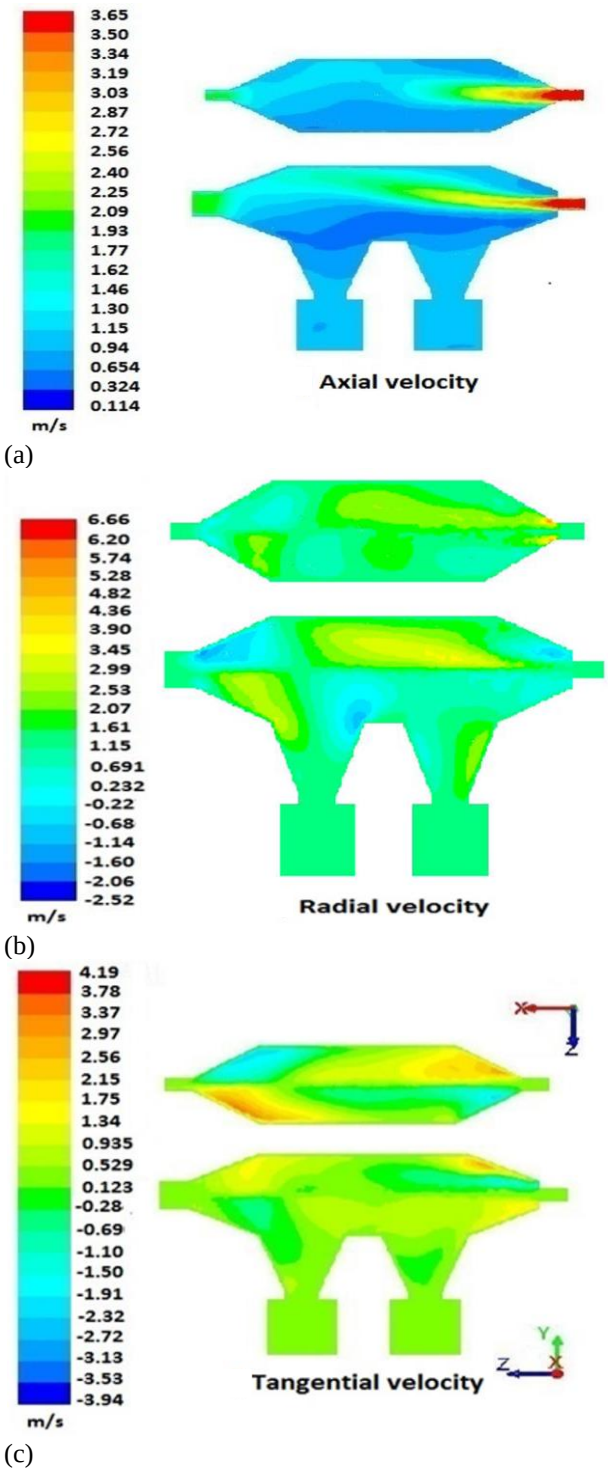

Fig. 7 Settling chamber velocity profiles (without baffle plate)

port. The axial velocity was found to be at its greatest at the convergent duct or outlet port. It implies that the particle pickup velocity was enhanced. Because of the increased pickup velocity, a greater number of particles escaped into the atmosphere. Furthermore, velocity at the dust collecting hoppers was lower than velocity at the settling chamber's top (Rectangular duct). It means that the particles' settling velocity was lower than their pickup velocity. According to the literature, it reduces the

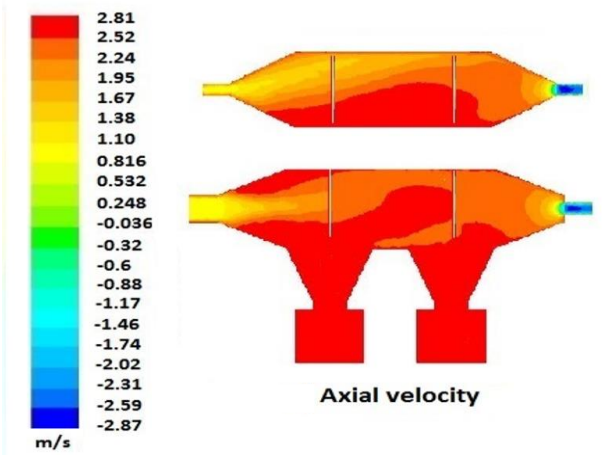

(a)

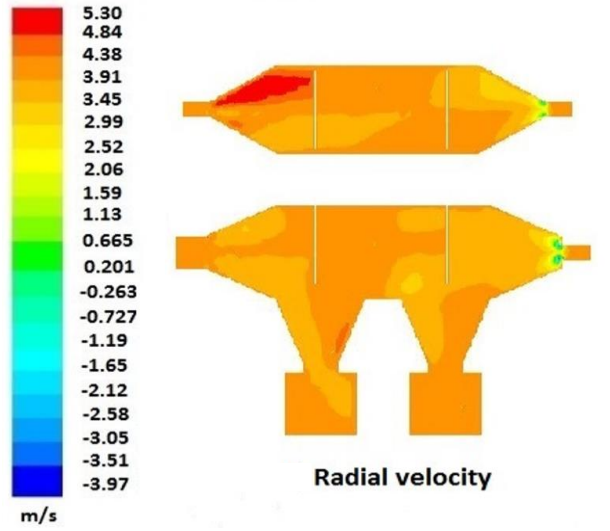

(b)

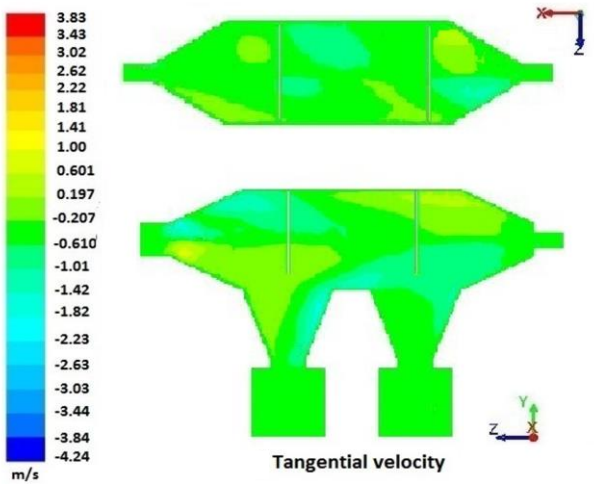

(c)

Fig. 8 Settling chamber velocity profiles (with baffle plate)

settling chamber's collection efficiency (Flagan & Seinfeld, 1988; Nasiri & Abdolzadeh, 2019; Kolaitis & Founti, 2002). When comparing Case 1 to the dust-collecting hoppers, the radial velocity was enhanced at the rectangular duct region. Furthermore, the radial velocity peaked towards the core of the convergent duct. It implies that the particle settling velocity was lower in the dust collection hoppers. The tangential velocity was increased in the wall location in Case 1. Furthermore, when compared to the upper half of the settling chamber, the tangential velocity was lower. It means that the particles that touched the dust collection hopper's wall were smaller. The axial velocity from the settling chamber intake to the outlet was lowered in Case 2 (with a baffle plate). When compared to the convergent part or exit port, the contour plots demonstrate that the axial velocity was high at the rectangular duct. It demonstrates that the particles are colliding with elevated rate in the baffle plate, and the flow direction has been deflected towards the dust collecting hoppers. In addition, the contours demonstrate that the axial velocity was greatest at the dust collection hoppers versus the rectangular duct region. It shows that the particles' terminal settling velocity has risen. According to the literature, increasing the settling velocity improves collecting efficiency (Flagan & Seinfeld, 1988; Nasiri & Abdolzadeh, 2019; Kolaitis & Founti, 2002). When compared to the convergent duct, the radial velocity was higher in the rectangular duct region. Moreover, due to the baffle plates, the radial velocity was high near the dust collection hoppers when compared to the rectangular region. In the baffle plate settling chamber, the radial velocity was increased at the wall region. It demonstrates that the settling velocity in the dust collection hoppers was increased. The tangential velocity is strong in the left side wall of the duct collection hopper 1 in Case 2. Tangential velocity was lowered at the right side wall of the duct collecting hopper 1. The tangential velocity was lower in the higher section of dust collecting hopper 2 than in the lower portion. It demonstrates that the particle pickup velocity was lowered. The velocity profiles were created in the X-Z plane at 900 mm (the beginning point of the convergent duct) from the entrance of the settling chamber, as shown in Fig. 9. In this plot, position zero was taken at the top of the duct. The velocity profiles of the baffle plate settling chamber demonstrate that the axial and radial velocities increase in the wall side as compared to the centre point. The axial and radial velocities were lower in the settling chamber wall region without a baffle plate (case 1). Furthermore, in Case 1, these velocities peaked in the centre of the settling chamber. In instances 1 and 2, the tangential velocity was raised from the centre towards the settling chamber's wall region. The results show that the baffle plate settling chamber has a higher settling velocity and a lower particle pickup velocity than the settling chamber without a baffle plate.

Figure 7a shows the axial velocity plot of the settling chamber without a baffle plate. As the flow enters the divergent duct, axial velocity decreases. Moreover, as it passed through the hopper, the air's axial velocity increased in the direction of the collection bin. Since the flow separation occurred from the rectangular chamber to the hopper, the axial velocity from the hopper to the bin varies from 0.324 m/s to 1.62 m/s. It indicates that the particles reach the bin with the highest settling velocity. On the other hand, Fig. 8a shows that the flow separation

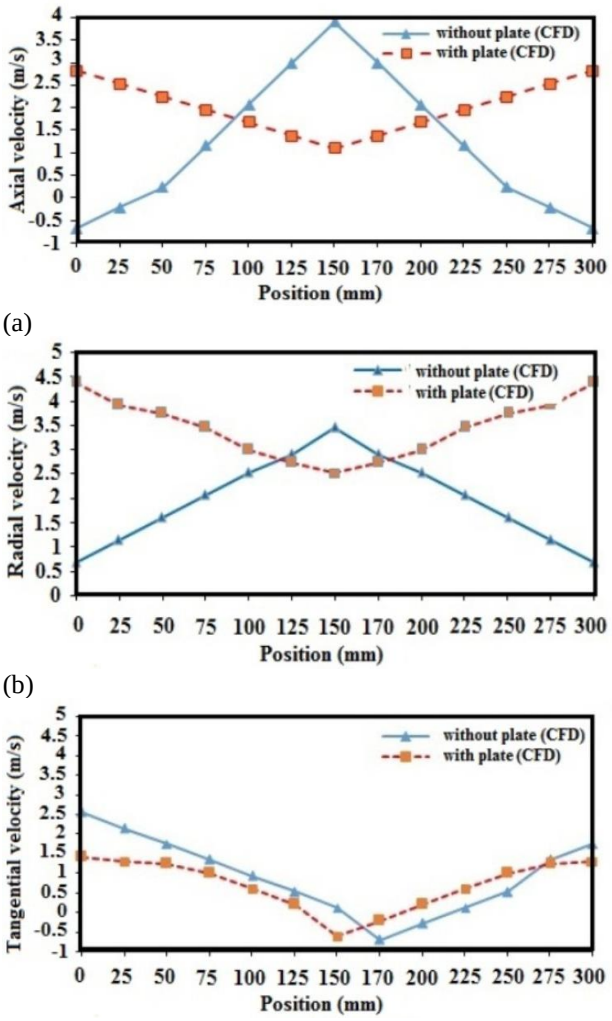

Fig. 9 Velocity profiles at 900 mm in X-Z plane

occurred due to the vertical baffle plate. Here, the baffle plates are kept 90° to the flow direction. Therefore, it creates an obstruction and a thin boundary layer in the flow path. It reduces the flow area and increases the axial velocity towards the bin. This contour ensures that the axial velocity varies from 1.1 m/s to 2.81 m/s. The introduction of baffle plates into the flow path caused the particles to reach the bin at a speed of 2.81 m/s. Figure 7b illustrates how the increase in rectangular cross-section area changes the flow rate when the flow enters the rectangular chamber from the divergent duct. This change in flow rate influences the radial velocity range. Furthermore, Fig. 8b demonstrates that the vertical baffle plate caused the radial velocity variation. Since the vertical baffle plates are kept near the hopper wall, it creates wall boundary layer separation. Moreover, the spacing between the two baffle plates is 355 mm. It creates a radial velocity variation from the rectangular chamber to the hopper. From the hopper wall to the rectangular chamber wall, the radial velocity varied from 2.99 m/s to 3.91 m/s. Figure 8c confirms that the tangential velocity variation occurred in the settling chamber wall region due to the baffle plate position and spacing. Furthermore, the duct geometry's expansion and contraction create a tangential velocity variation. This expansion and contraction of the duct creates turbulence

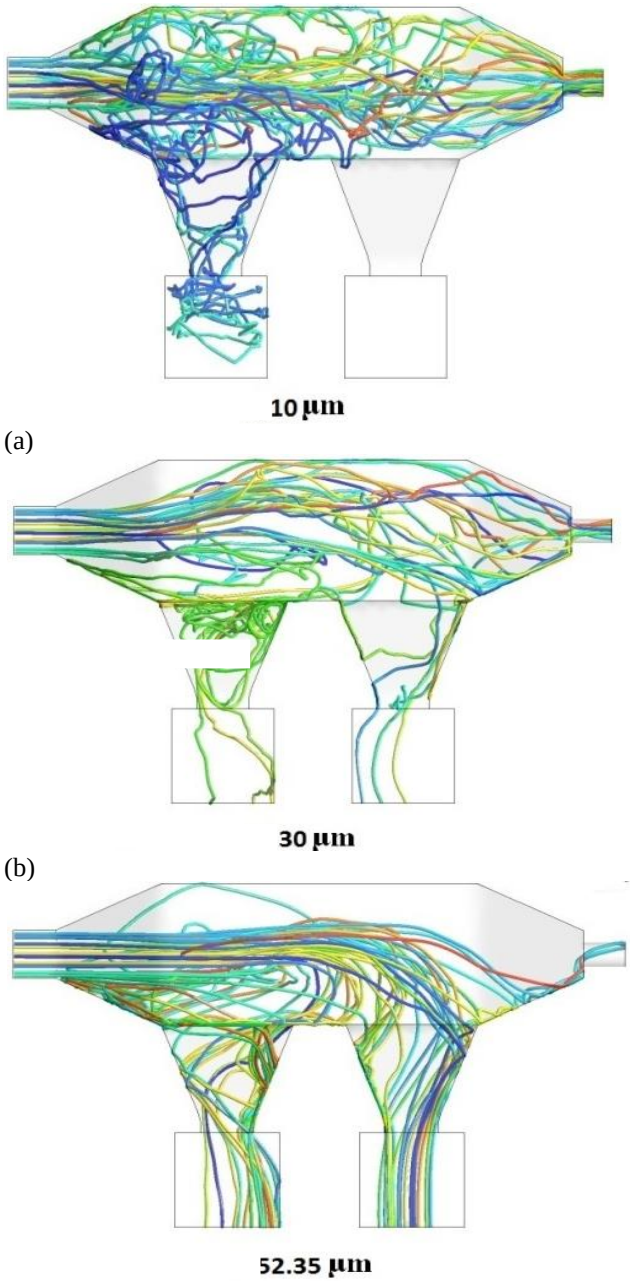

Fig. 10 Settling chamber particle flow pattern for without baffle plate a) 10 µm b) 30 µm c) 52.35 µm

and boundary layer separation in the wall region. Therefore, the hopper wall region has high tangential velocity. From the settling chamber wall region to the centre, the tangential velocity varies from 1.81 m/s to 0.197 m/s. It forces the particles to hit the settling chamber's wall.

5.3 Particle Flow Pattern Results

The particle trajectories obtained at 2.5 m/s through the DPM are shown in Figs 10 and 11. In CFD analysis, the particle flow pattern tracking lines are indicated by the rainbow colors. Just these colours indicate the flow path lines (these colours do not differentiate anything in the simulation result). Those trajectory lines indicate how the particles are settling in the collection bin and escaping to the atmosphere through the outlet port.

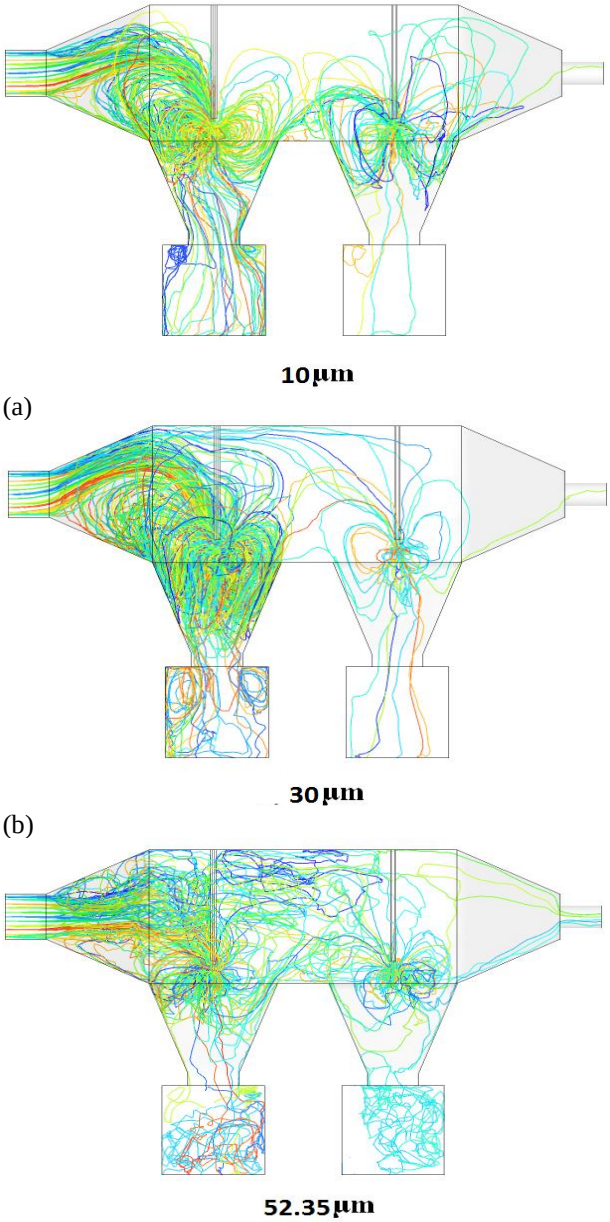

Fig. 11 Settling chamber particle flow pattern for with baffle plate a) 10 µm b) 30 µm c) 52.35 µm

Moreover, these trajectory lines show the flow diversion due to the baffle plates in the settling chamber. In case 1 (without baffle plate), when 10 µm size of particles are introduced at the settling chamber's inlet, only a few particles agglomerate on the first hopper. The settling chamber efficiency was 5% at 10 µm (without baffle plate). The trajectory indicates that a few particles settled at the first collection bin. On the other hand, none of the particles reach the second hopper and its collection bin. Most of the particles escaped through the settling chamber outlet. In case 2 (with baffle plate), the settling chamber efficiency was 7% at 10 µm. The trajectory shows that few particles settled at the first collection bin, and few particles settled at the second collection bin. It was observed that more particles agglomerated in the first hopper compared to the second hopper. It indicates that the terminal settling velocity of particles was increased due to the first baffle plate.

In case 1, the settling chamber's first collection bin collected more particles compared to the second bin when 30µm particles were injected. The settling chamber efficiency was 13% at 30µm. In case 2, the settling chamber's first collection bin collected more particles compared to the second bin. Moreover, the highest number of particles agglomerates on the first hopper compared to the second hopper. The predicted efficiency was 18% at 30µm. In case 1, the efficiency of the settling chamber was 25% at 52.35 µm. The trajectory shows that the two collection bins collected very few particles. In case 2, the first collection bin of the settling chamber collected more particles compared to the second one. In this work, collection efficiencies of 10 µm and 30 µm particles are simulated in CFD analysis alone. Since preparing all the particles for the ball milling process is a costly and time-consuming process, Therefore, only the 52.35 µm particles have been prepared, and they were tested in experimental analysis, and the correctness of the simulation results were compared with this case alone. In case 2, the settling chamber efficiency is 43% (CFD). The particle flow pattern results indicate that the setting chamber's first collection bin collected more particles. Furthermore, the settling chamber's second collection bin collected fewer particles. In this work, the experimental setup has been created with a baffle plate. The experimental results reveal the same. The process of ball milling prepares the particles. The average size of the particles obtained is 52.35 µm. The experimental results (with a baffle plate) show that the settling chamber collected 96 g of particles out of 200 g of particles injected at 52.35 µm. It was observed that 74 g of particles were settled in the first collection bin, and 22 g of particles were collected in the second collection bin. Two collection bins collected 96 g of particles at 2.5 m/s, with the remaining 104 g escaping to the atmosphere through the blower outlet port. The efficiency of the baffle plate settling chamber was 45% in the experimental investigation at 52.35 µm. In CFD analysis, the settling chamber efficiency was 43%. The variation between the experimental and CFD results was 4.4%.

In case 1, injecting 10 µm-sized particles at the settling chamber's inlet (without a baffle plate) resulted in a few particles settling in the first bin and no particles in the second bin. According to Eq. 2, the terminal settling velocity is directly proportional to the particle diameter. At 10 µm, the estimated terminal settling velocity is 0.01 m/s. It is extremely low, and it increases the particles' residence time inside the chamber. Furthermore, the rectangular chamber is 0.6 m long, and the total length from the inlet to the outlet is 1.2 m. As a result, the particle's travel or residence time increases. Furthermore, this leads to a decrease in the settling velocity in the second hopper and bin regions. Moreover, small particles have a high residence time due to the turbulence. Therefore, the second bin does not settle the particles. On the other hand, in case 2 (baffle plate chamber), the estimated settling velocity is 0.04 m/s at 10 µm. The baffle plate boosts the settling velocity. Furthermore, the divergent duct reduces the flow velocity, thereby reducing the particle's kinetic energy. In addition, the baffle plate creates an obstruction in the

flow path and creates a thin boundary layer. It shortens particles' residence time. As a result, the flow diverts to the first hopper, which has an increased settling velocity. As a result, the more particles settled in the first bin, the higher the number of particles agglomerated in the first hopper. At the same time, a few particles escaped from the first bin due to their pickup velocity. The particles collided with the second baffle plate, causing the flow to diverge once more due to the obstruction and boundary layer formation. As a result, the particles experienced a further decrease in kinetic energy, causing a few particles to settle in the second bin.

Figures 10b and 11b demonstrate the settling of a few particles in both the first and second bins. According to Eq. 2, a larger particle diameter increases the terminal settling velocity. Without the baffle plate chamber, the estimated settling velocity is 0.11 m/s at 30 µm. Compared to the previous study, the settling velocity has increased. As well, the settling velocity is 0.32 m/s at 30 µm for the baffle plate chamber. It shows that the settling velocity increased three times when compared to case 1. Consequently, the particles settled in both bins. Compared to previous cases, Figs 10c and 11c demonstrate a higher number of particles settling in the collection bin. The settling velocity is 0.32 m/s at 52.35 µm without the plate chamber, and it is 0.96 m/s at 52.35 µm for the baffle plate chamber. Moreover, the flow pattern lines indicate that a greater number of particles travelled between the two baffle plates. It reduces the particles' kinetic energy and settling time. As a result, the baffle plate settling chamber's performance improves.

Figure 12 shows the results of particle size versus settling velocity. This plot clearly reports that the settling velocity increases with increasing particle size. The baffle plate settling chamber exhibits a higher settling velocity compared to a chamber without a baffle plate. The introduction of a baffle plate between the flow paths creates an obstruction and alters the chamber's cross section. As a result, a thin boundary layer forms in the chamber's wall region, causing turbulence inside. As a result, the particles' settling velocity increases. At 150 µm, the maximum settling velocity of the particles with and without baffle plate cases is 8.07 m/s and 2.69 m/s, respectively. It shows that the particles' settling velocity is 66.6% higher when the baffle pate is introduced in flow paths.

Figure 13 reports the details of settling velocity versus settling time. In this analysis, we measured the variations in settling velocity from the rectangular chamber to the bottom of the collection bin in Figs 7 and 8. Without the baffle plate case, the settling velocity varied from 0.324 m/s to 1.62 m/s from the hopper to the bin. In this case, the particle reach time decreases from 0.93 s to 0.19 s. The settling velocity increased from 1.1 m/s to 2.81 m/s in the baffle plate case. In this case, we varied the particle reach time from 0.27 s to 0.11 s. It was observed that the particle reach time or settling time is reduced when increasing the settling velocity. As previously discussed, a larger particle size increases the settling velocity. An increase in settling velocity also reduces settling time. This result clearly demonstrates

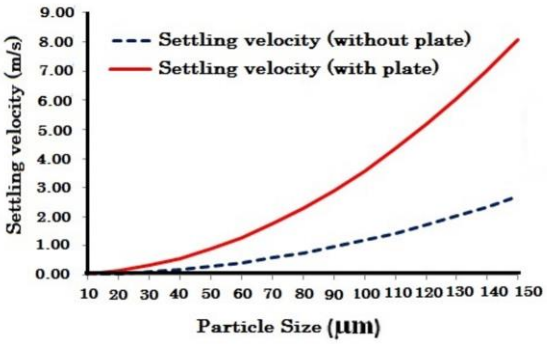

Fig. 12 Particle size (µm) vs settling velocity (m/s)

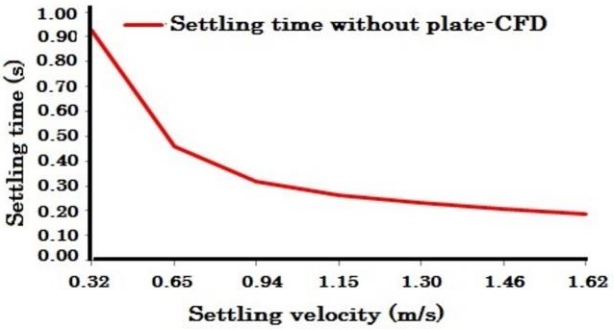

(a)

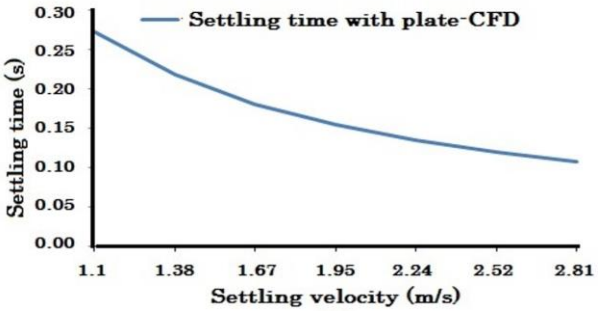

(b)

Fig. 13 Settling velocity (m/s) vs settling time (s) a) without baffle plate b) with baffle plate

that larger particles take less time to settle and smaller particles take longer to reach the bin. The baffle plate setting chamber has a shorter particle reach time when compared to the chamber without baffle plates. Therefore, it collects more particles.

5.4 Settling Chamber Efficiency

The settling chamber efficiency for the dissimilar particle sizes is exposed in Fig. 14. It shows that the case 1 and case 2 settling chambers have not collected any particles up to 9 µm. Those settling chambers collected particles in their collection bins of 10 µm particle size. In case 1, the settling chamber reached maximum collection efficiency at 150 µm. In case 2, the settling chamber reached maximum collection efficiency at 100 µm. In case 1, the settling chamber collection efficiency was 68% at 100 µm. It indicates that the settling chamber efficiency increased by 32% when baffle plates were

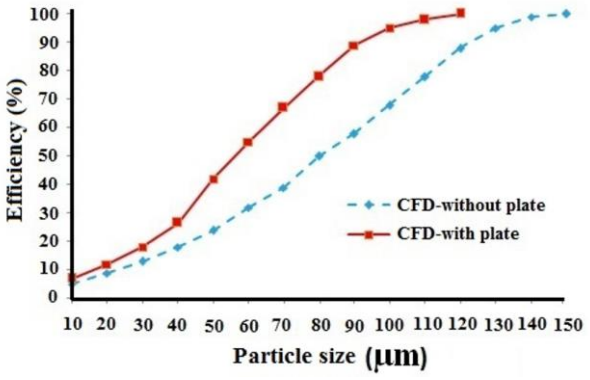

Fig. 14 Settling chamber efficiency plot for different size of particles

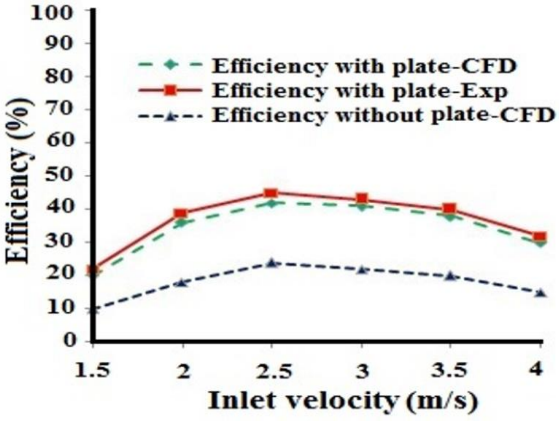

Fig. 15 Settling chamber efficiency (at 52.35 µm) plot for different inlet velocities

introduced between the flow paths. The efficiency of the baffle plate settling chamber was 45% in experimental investigation at 52.35 µm. In CFD analysis, the settling chamber efficiency was 43%. The variation between the experimental and CFD results was 4.4%. At the same particle size, the competence of the settling chamber in the first case was 25% (CFD). The data reveal that case 2 was 44.4% more efficient than instance 1.

Figure 15 depicts the settling chamber efficiency for various inlet velocities at a particle size of 52.35 µm. This graphic illustrates that increasing the particle inlet velocity to 2.5 m/s improves the settling chamber efficiency. The findings demonstrate that raising the intake velocity above 2.5 m/s reduces collecting efficiency. Because it raises the particle's pickup velocity. As a result, more particles depart the settling chamber through the exit nozzle. Table 3 displays the

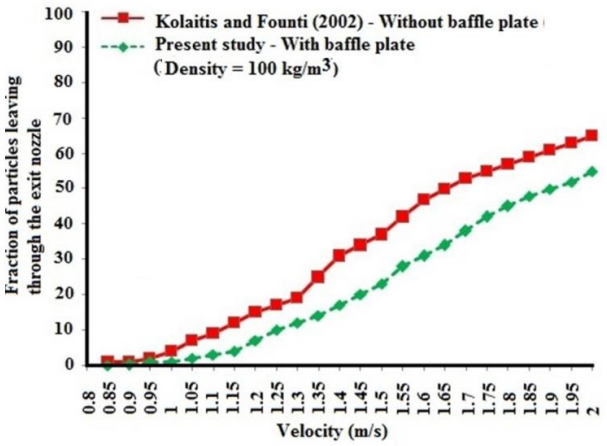

Fig. 16 Comparison Velocity vs Fraction of particles escaped to the exit nozzle

comparison results. Without the baffle plate casing, the settling chamber cut-off diameter was 80 µm. In addition, the baffle plate case had a cut-off diameter of 57 µm. It demonstrates that when particle sizes exceed 57 µm, the baffle plate chamber performs better.

Kolaitis and Founti (2002) predicted the fraction of particles that escaped through the exit nozzle in the settling chamber for various inlet velocities (without baffle plate). In that study, the density of particles considered for analysis was 100 kg/m^3. The results show that the increment in velocity increases the fraction of particles that escape through the exit nozzle. It was found that 65% of the particles escaped through the exit of the nozzle at a velocity of 2 m/s. The particle used in that study was 2.5 mm in size. Fig. 16 depicts the comparing results. In this investigation, the same parameters were used to evaluate the performance of the baffle plate settling chamber. The present study reports that the fraction of particles that escaped to the exit nozzle was 54%. It indicates that the baffle plate settling chamber efficiency was 11% higher than the previous model when the density was 100 kg/m^3. Further, the study reports that the density and velocity of the particle play a major role in the collection efficiency. The experimental study reports that the velocity of the particles must increase when their density is high. As well, the velocity of the particles must decrease when the density of the particles is low. In this experimental analysis, three trials have been conducted to predict the settling chamber pressure drop and efficiency. Based on those three test data points, the error bar is plotted for the inlet velocity vs. pressure drop and the inlet velocity vs. efficiency, which is shown

Table 3 Settling chamber comparison results in 2.5 m/s velocity

Cases	Δp (N/m^2) CFD	Δp (N/m^2) Experiment	Cut-off diameter (µm) CFD	Efficiency (%) at (52.35 µm)-CFD	Efficiency (%) at (52.35 µm) Experiment
Without baffle plate	135.4	-	80	25	-
With baffle plate	141.6	147.1	57	43	45

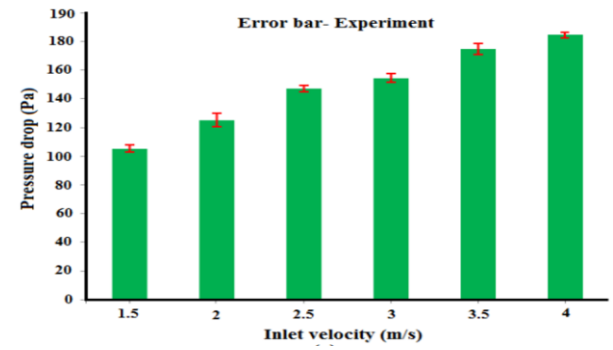

(a)

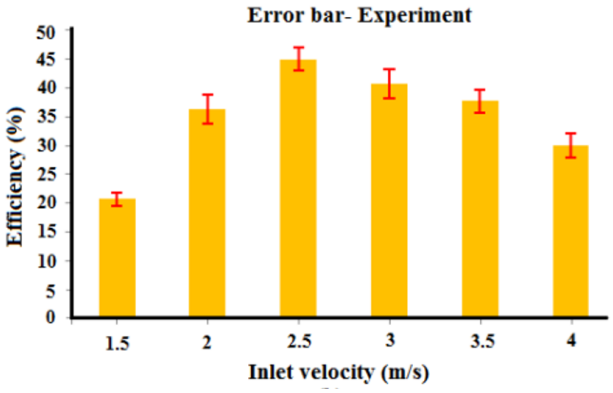

(b)

Fig. 17 a) Error bar pressure drop vs inlet velocity b) Error bar efficiency vs inlet velocity

in Figure 17. The error bar report shows that the maximum standard deviation for the pressure drop results is 4.55. As well, the maximum standard deviation for the efficiency result is 2.52.

6. CONCLUSION

In this work, two types of settling chambers were considered for analysis. Case 1 was considered without a baffle plate, and case 2 was considered with a baffle plate. The CFD simulation was carried out to predict the particle trajectories and flow characteristics of the above-mentioned setting chambers. The following points have been observed during the investigation:

- It was found that a thin boundary layer was formed when introducing the baffle plate inside the settling chamber. It creates turbulence in the hopper region which increases the settling velocity.
- It was noted that at 150 µm, the maximum settling velocity of the particles with and without baffle plate cases is 8.07 m/s and 2.69 m/s, respectively.
- It shows that the particles' settling velocity is 66.6% higher when the baffle pate is introduced in flow paths.
- It was observed that the maximum settling velocity is 1.62 m/s for without baffle plate case. Moreover, it is 2.81 m/s for baffle plate case.
- The wave is created between the plate and convergent duct due to the first baffle plate. Therefore, the flow is redirected towards the hoppers and dust bin at a high terminal settling velocity.
- Placing the baffle plate in the flow route increases the pressure drop marginally. At 2.5 m/s, the pressure drop in the baffle plate settling chamber was 141.6 Pa. The pressure drop at 2.5 m/s was 135.4 Pa without the baffle plate settling chamber. The experimental results show that the pressure drop at 2.5 m/s (with baffle) was 147.1 Pa (15 mm of H2O). The deviation between experiment and CFD results is 3.8% for the baffle plate chamber.
- The vertical baffle plate creates wall boundary layer separation in the chamber. Therefore, a radial velocity variation was occurred from the rectangular chamber to the hopper. From the hopper wall to the rectangular chamber wall, the radial velocity varied from 2.99 m/s to 3.91 m/s. At the same time, the tangential velocity varies from 1.81 m/s to 0.197 m/s due this baffle plate. It forces the particles to hit the settling chamber's wall. Therefore, baffle plate chamber collected more particles.
- It was observed that setting velocity is increased when increasing the particle size. Moreover, increment in the settling velocity increases the particle reach time or settling time. It reduces the residence time of the particles. The minimum particle reach time for the without baffle plate settling chamber is 0.19 s. The minimum particle reach time for the with baffle plate settling chamber is 0.11 s.
- It concludes that larger particles take less time to settle and smaller particles take longer time to reach the bin. The baffle plate setting chamber has a shorter particle reach time when compared to the chamber without baffle plates. Therefore, it collects more particles.
- In both cases, the settling chamber pressure was increased from the inlet section to the exit nozzle. The settling chamber has less pressure drop in collection bins compared to the rectangular duct in both cases.
- The baffle plate settling chamber has a high settling velocity and a lower pickup velocity of the particle compared to the settling chamber without a baffle plate. It indicates that the baffle plate settling chamber has high collection efficiency.
- The collection efficiency of the baffle plate settling chamber was 43% (CFD result) at 52.35µm. The experimental result shows that the baffle plate settling chamber collected 45 % of particles at the above-mentioned particle size.
- As well, the settling chamber without a baffle plate collected 25% of particles at 52.35 µm. The efficacy of the baffle plate settling chamber was 44.4% higher than the case 1. Moreover, the settling chamber efficiency decreased after 2.5 m/s particle velocity in both cases.

ACKNOWLEDGEMENT

This work is sponsored by DST-FIST 2022, Government of India. The grant number is SR/FST/COLLEGE-/2022/1300.

CONFLICT OF INTEREST

The authors declare that they have no known competing financial interests or personal relationships that could have appeared to influence the work reported in this paper.

AUTHORS CONTRIBUTION

S. Venkatesh: Experiment, Conceptualization, Methodology, Funding acquisition, Writing – original draft. **R. Krishnaraj:** Conceptualization. **P.M.Gopal:** Writing – review & editing**, V.Kavimani:** Writing – review & editing.

DATA AVAILABILITY

The data used to support the findings of this study are included within the article.

REFERENCES

Bhattacharjee, R. C. (2003). Optimal design of a settling chamber-an air pollution control device. *WIT Transactions on Ecology and the Environment*, *66*. 1-10. https://doi.org/ 10.2495/AIR030521

Chuah, T. G., Gimbun, J., & Choong, T. S. (2006). A CFD study of the effect of cone dimensions on sampling aerocyclones performance and hydrodynamics. *Powder Technology*, *162*(2), 126-132. https://doi.org/10.1016/j.powtec.2005.12.010

Elsayed, K., & Lacor, C. (2010). Optimization of the cyclone separator geometry for minimum pressure drop using mathematical models and CFD simulations. *Chemical Engineering Science*, *65*(22), 6048-6058. https://doi.org/10.1016/j.ces.2010.08.042Get rights and content

Elsayed, K., & Lacor, C. (2012). The effect of the dust outlet geometry on the performance and hydrodynamics of gas cyclones. *Computers & Fluids*, *68*,134-147. https://doi.org/10.1016/j.compfluid.2012.07.029

Fatahian, H., Fatahian, E., & Nimvari, M. E. (2018). Improving efficiency of conventional and square cyclones using different configurations of the laminarizer. *Powder Technology*, *339*, 232-243. https://doi.org/10.1016/j.powtec.2018.08.038

Feather, G. A., & Chen, B. T. (2003). Design and use of a settling chamber for sampler evaluation under calm-air conditions. *Aerosol Science & Technology*, *37*(3), 261-270. https://doi.org/10.1080/02786820300946

Flagan, R. C., & Seinfeld, J. H. (1988). *Removal of particles from gas streams. Fundamentals of Air Pollution Engineering*. Prentice-Hall, Inc., Englewood Cliffs, NJ.

Fluent, Inc., Fluent 6.1.22 Users' Guide. (2004).

Griffiths, W. D., & Boysan, F. (1996). Computational fluid dynamics (CFD) and empirical modelling of the performance of a number of cyclone samplers. *Journal of Aerosol Science*, *27*(2), 281-304. https://doi.org/10.1016/0021-8502(95)00549-8

Houben, J. J. H., Weiss, C., & Brunnmair, E. (2016). CFD simulations of pressure drop and velocity field in a cyclone separator with central vortex stabilization rod. *Journal of Applied Fluid Mechanics*, *9*(1), 487-499. https://doi.org/10.18869/ACADPUB.JAFM.68.224.23934

Kolaitis, D. I., & Founti, M. A. (2002). Modeling of the gas–particle flow in industrial classification chambers for design optimization. *Powder Technology*, *125*(2-3), 298-305. https://doi.org/10.1016/S0032-5910(01)00518-6

Launder, B. E., & Shima, N. (1989). Second-moment closure for the near-wall sublayer-development and application. *AIAA Journal*, *27*(10), 1319-1325. https://doi.org/10.2514/3.10267

Launder, B. E., & Spalding, D. B. (1983). *The numerical computation of turbulent flows.* Numerical prediction of flow, heat transfer, turbulence and combustion (pp.96-116). Pergamon. https://doi.org/10.1016/B978-0-08-030937-8.50016-7

Liu, X., Zhang, Y., Wu, Q., Zhang, M., Liu, F., & Guo, Y. (2019). Study on the key structure parameters of a gravity settling chamber based on a flow field simulation. *Engineering Applications of Computational Fluid Mechanics*, *13*(1), 377-395. https://doi.org/10.1080/19942060.2019.1595729

Morsi, S. A. J., & Alexander, A. J. (1972). An investigation of particle trajectories in two-phase flow systems. *Journal of Fluid Mechanics*, *55*(2), 193-208. https://doi.org/10.1017/S0022112072001806

Nasiri, A., & Abdolzadeh, M. (2019). Effect of baffle arrangement and inlet air velocity on particulate removal efficiency of a gravitational settling chamber in a coke-making plant. *International Journal of Coal Preparation and Utilization* 39، 347-372. https://doi.org/10.1080/19392699.2017.1333114

Nieto, P. G., del Coz Díaz, J. J., Castro-Fresno, D., & Muñoz, F. B. (2010). Numerical simulation of the performance of a snow fence with airfoil snow plates by FVM. *Journal of Computational and Applied Mathematics*, *234*(4),1200-1210. https://doi.org/10.1016/j.cam.2009.07.048

Patro, B., Kupireddi, K. K., & Devanuri, J. K. (2023).

Heat transfer and pressure drop studies of vertical gas-particle flow using a variable gas property two-fluid model. *Iranian Journal of Science and Technology, Transactions of Mechanical Engineering*, *47*(3),893-903. https://doi.org/10.1007/s40997-022-00561-6

Rajmistry, S., Ganguli, S., Chandra, P., Karmakar, M. K., & Chatterjee, P. (2017). Numerical analysis of gas-solid behavior in a cyclone separator for circulating fluidized bed system. *Journal of Applied Fluid Mechanics*, *10*(4), 1167-1176. https://doi.org/10.18869/acadpub.jafm.73.241.26951

Raoufi, A., Shams, M., & Kanani, H. (2009). CFD analysis of flow field in square cyclones. *Powder Technology*, *191*(3),349-357. https://doi.org/10.1016/j.powtec.2008.11.007

Roache, P. J. (1994). Perspective: a method for uniform reporting of grid refinement studies. *Journal of Fluids Engineering*, *116*, 405-413. https://doi.org/10.1115/1.2910291

Romblad, J., Greiner, M., Guissart, A., & Würz, W. (2022). Characterization of low levels of turbulence generated by grids in the settling chamber of a laminar wind tunnel. *Experiments in Fluids*, *63*(4), 65. https://doi.org/10.1007/s00348-022-03418-5

Safikhani, H., Akhavan-Behabadi, M. A., Nariman-Zadeh, N., & Abadi, M. M. (2011a). Modeling and multi-objective optimization of square cyclones using CFD and neural networks. *Chemical Engineering Research and Design*, *89*(3), 301-309. https://doi.org/10.1016/j.cherd.2010.07.004

Safikhani, H., Shams, M., & Dashti, S. (2011b). Numerical simulation of square cyclones in small sizes. *Advanced Powder Technology*, *22*(3), 359-365. https://doi.org/10.1016/j.apt.2010.05.003

Sahmel, J., Avens, H. J., Scott, P. K., Unice, K., Burns, A., Barlow, C. A., & Paustenbach, D. J. (2015). Measured removal rates of chrysotile asbestos fibers from air and comparison with theoretical estimates based on gravitational settling and dilution ventilation. *Inhalation Toxicology*, *27*(14), 787-801. https://doi.org/10.3109/08958378.2015.1110216

Sinnott, R. (2005). *Chemical engineering design: chemical engineering. Volume 6*. Elsevier.

Slack, M. D., Prasad, R. O., Bakker, A., & Boysan, F. (2000). Advances in cyclone modelling using unstructured grids. *Chemical Engineering Research and Design*, *8*(78), 1098-1104. https://doi.org/10.1205/026387600528373

Su, Y., Zheng, A., & Zhao, B. (2011). Numerical simulation of effect of inlet configuration on square cyclone separator performance. *Powder Technology*, *210*(3), 293-303. https://doi.org/10.1016/j.powtec.2011.03.034

Venkatesh, S., & Sakthivel, M. (2017). Numerical investigation and optimization for performance analysis in Venturi inlet cyclone separator. *Desalination and Water Treatment*, *90*, 168-179. https://doi.org/10.5004/dwt.2017.21444

Venkatesh, S., Sivapirakasam, S. P., Sakthivel, M., Krishnaraj, R., & Leta, T. J. (2021). Investigation on hydrocyclone for increasing the performance by modification of geometrical parameters through cfd approach. *Desalin. Water Treat*, *244*, 157-166. https://doi.org/10.5004/dwt.2021.27944

Wasilewski, M., Brar, L. S., & Ligus, G. (2020). Experimental and numerical investigation on the performance of square cyclones with different vortex finder configurations. *Separation and Purification Technology*, *239*,116588. https://doi.org/10.1016/j.seppur.2020.116588

Zhao, B., Su, Y., & Zhang, J. (2006). Simulation of gas flow pattern and separation efficiency in cyclone with conventional single and spiral double inlet configuration. *Chemical Engineering Research and Design*, *84*(12),1158-1165. https://doi.org/10.1205/cherd06040